Multiphoton Ionization Reduction of Atoms in Two-Color Femtosecond Laser Fields

Hong-Bin Yao,[1,2] Qi-Wen Qu,[3] Zhao-Han Zhang,[1] Jia-Wei Wang,[3] Jian Gao,[3,4] Chen-Xi Hu,[1] Hui Li,[3,*] Jian Wu,[3,4,5] and Feng He[1,5,†]

[1]*Key Laboratory for Laser Plasmas (Ministry of Education) and School of Physics and Astronomy, Collaborative innovation center for IFSA (CICIFSA), Shanghai Jiao Tong University, Shanghai 200240, China*

[2]*Key Laboratory of New Energy and Materials Research of Xinjiang Education Department, Xinjiang Institute of Engineering, Urumqi 830091, China*

[3]*State Key Laboratory of Precision Spectroscopy, East China Normal University, Shanghai 200241, China*

[4]*Chongqing Key Laboratory of Precision Optics, Chongqing Institute of East China Normal University, Chongqing 401121, China*

[5]*CAS Center for Excellence in Ultra-intense Laser Science, Shanghai 201800, China*

(Received 4 October 2022; accepted 23 February 2023; published 14 March 2023)

We report the ionization reduction of atoms in two-color femtosecond laser fields in this joint theoretical-experimental study. For the multiphoton ionization of atoms using a 400 nm laser pulse, the ionization probability is reduced if another relatively weak 800 nm laser pulse is overlapped. Such ionization reduction consistently occurs regardless of the relative phase between the two pulses. The time-dependent Schrödinger equation simulation results indicate that with the assisted 800 nm photons the electron can be launched to Rydberg states with large angular quantum numbers, which stand off the nuclei and thus are hard to be freed in the multiphoton regime. This mechanism works for hydrogen, helium, and probably some other atoms if two-color laser fields are properly tuned.

DOI: 10.1103/PhysRevLett.130.113201

Ionization is a cornerstone for many fundamental processes in light-matter interaction, such as high harmonic generation [1–3], laser-assisted electron-ion recollision [4], reconstruction of target structures [5], and molecular dissociation [6–8]. The recognition of atomic ionization undergoes several stages. Before the invention of lasers, Einstein claimed that the photon energy must be larger than the ionization potential to produce photoelectrons. Such a constraint was broken with the advent of strong laser technologies. In strong field physics, according to the Keldysh parameter [9], different laser conditions bring different ionization scenarios. If the Keldysh parameter is larger than one, an electron simultaneously absorbs multiple photons and conquers the ionization potential [10]. On the other hand, if the Keldysh parameter is smaller than one, the laser field severely bends the Coulomb potential and forms a barrier, through which an electron may tunnel out [11,12].

Ionization can be controlled by constructing different laser fields [13–16]. Among all strategies, two-color femtosecond laser fields have been extensively used, which are well-developed with robust freedoms to be tuned. Experimentally, two-color laser pulses are usually composed of a strong 800 nm fundamental wave (FW) and its 400 nm second harmonic (SH) [17–19]. The strong FW determines the main interaction picture, and the weak SH perturbs interaction processes. Such a strategy has been implemented to streak intracycle interference of electron wave packets [20], to construct a phase-of-phase spectroscopy [21] which can be used to extract the time delay of photoelectron emission with the accuracy of attoseconds [22]. In these studies based on two-color laser fields, the relative phase of the two frequencies is a key parameter to be tailored. Depending on the relative phase, different ionization pathways may constructively or destructively interfere with each other, leading to the phase-resolved photoelectron-yield fluctuation [21–23]. Consequently, it seems impossible for the homogeneous ionization reduction to take place regardless of the relative phase. However, such a preconception breaks in this study. Besides the relative phase, the relative intensity of two-color laser pulses works as another knob to manipulate photoionization processes [24,25]. While usually a strong FW plus a weak SH is extensively applied, a strong SH plus a relatively weak FW has been used to measure photoionization time delays and the phase shifts in the above threshold ionization (ATI) [26–31]. Nevertheless, ionization reduction has not been reported though it fundamentally determines the subsequent ionization-induced dynamics.

In this Letter, we report a unique mechanism of atomic ionization reduction in two-color laser fields. Taking hydrogen and helium atoms as prototypes, we investigate their ionization in the two-color fields by overlapping a strong SH with another relatively weak FW. While the sole SH initiates the multiphoton ionization, the addition of a relatively weak FW pulse consistently inhibits the ionization regardless of the relative phase between the SH and

FW pulses. By tracing intermediate states and resolving the photoelectron wave packets to the components with different angular quantum numbers, we found that the FW assists the electronic transition to Rydberg states with large angular quantum numbers, which are hard to be ionized in the multiphoton ionization regime. The prediction based on the time-dependent Schrödinger equation (TDSE) is confirmed by experimental measurements applied on He atoms.

The TDSE for the laser-atom interaction in the velocity gauge can be written as (atomic units $e = \hbar = m = 1$ are used throughout unless otherwise stated)

$$i\frac{\partial}{\partial t}\Psi(\mathbf{r},t) = \left[-\frac{\nabla^2}{2} + V(r) - i\mathbf{A}(t)\cdot\nabla\right]\Psi(\mathbf{r},t), \quad (1)$$

where $V(r) = -1/r$ for hydrogen and $V(r) = -(1 + 1.231e^{-0.662r} - 1.325re^{-1.236r} - 0.231e^{-0.48r})/r$ for helium in the single-active-electron approximation [32], and the linearly polarized laser vector potential $A(t)$ is

$$A(t) = f(t)\left[-\frac{E_{\mathrm{SH}}}{\omega_{\mathrm{SH}}}\sin(\omega_{\mathrm{SH}}t) - \frac{E_{\mathrm{FW}}}{\omega_{\mathrm{FW}}}\sin(\omega_{\mathrm{FW}}t + \phi)\right]. \quad (2)$$

Here, ω_{SH} and ω_{FW} are the angular frequencies of the SH and FW, E_{SH} and E_{FW} are the electric field amplitudes of SH and FW, and the pulse envelop $f(t) = \sin^2(\pi t/T_p)$ is adopted with the duration of $T_p = 20T_{\mathrm{SH}}$ with T_{SH} the optical period of the SH. The relative phase of the two fields is denoted by ϕ.

Numerically, the wave function $\Psi(\mathbf{r},t)$ is expanded with the basis of B-spline functions [33] and spherical harmonics in the finite element representation. The initial wave function is obtained by diagonalizing the field-free Hamiltonian, and the time propagation of a wave function is performed by the Crank-Nicolson method with a corresponding split-operator technique [34–36]. The TDSE is solved in a spherical box of the size $r_{\max} = 1500$ a.u. with the time step $\Delta t = 0.008$ a.u.. The excitation probability to a (n, l) state is extracted by projecting the wave function onto the field-free quantum states, where n ($n > 1$) and l are the principle quantum number and the angular quantum number. Summing over all these populations, we obtain the total excitation probability. The total ionization probability and photoelectron energy spectra (PES) are extracted at the end of simulations by projecting the final wave function onto the continuum states of the field-free Hamiltonian [33,37]. We yield converged results using the number of partial waves $l = 40$ with $1500B$-spline functions.

By fixing the SH intensity, we calculate the ionization probabilities as a function of the FW intensity. Results are shown in Figs. 1(a) and 1(b) for hydrogen and helium atoms, respectively. The red bullets and error bars denote the averaged ionization probabilities and the corresponding dispersion over the relative phases $0 \le \phi < 2\pi$. Regardless

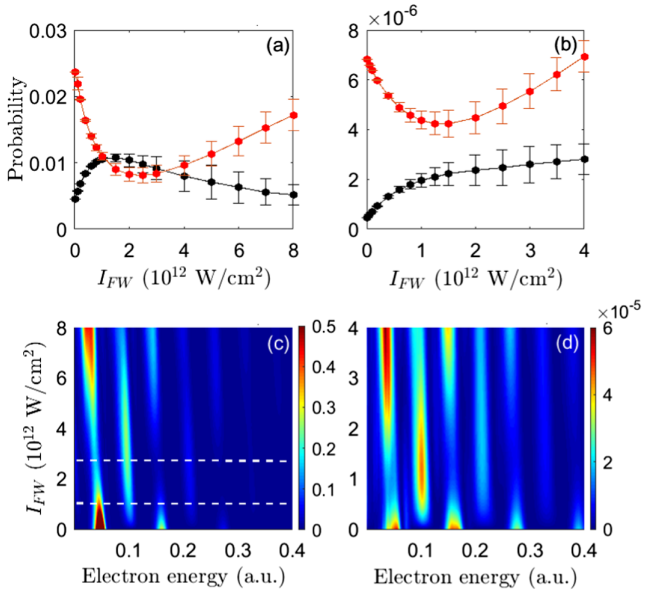

FIG. 1. Upper row: the ionization (red lines) and excitation (black lines) probabilities as a function of I_{FW} for hydrogen (a) and helium (b). Lower row: the I_{FW}-dependent PES for hydrogen (c) and helium (d). The SH intensity is fixed at $I_{\mathrm{SH}} = 5 \times 10^{13}$ W/cm^2 for hydrogen and 1.5×10^{14} W/cm^2 for helium. The ϕ-averaged probabilities over the range $0 \le \phi < 2\pi$ are indicated by the bullets, and the error bars denote the probability dispersion when ϕ varies. The horizontal dashed lines divide the spectrogram into several parts to be discussed in Fig. 2 and Fig. 3.

of ϕ, ionization probabilities are homogeneously reduced when adding the FW on top of the SH, which is beyond one's expectation. For reference, the excitation probabilities are also presented in black. The sum of the ionization probability and excitation probability varies dully with the FW intensity, which suggests that this total probability is mainly determined by the sole SH and the FW simply allots the population between the bound and continuum states. The sole FW nearly cannot excite the atom, which has been confirmed by turning off the 400 SH in simulations. For the laser parameters used in this study, the total excitation and ionization probabilities are much smaller than one, and thus the ground state depletion is negligible.

Since ϕ does not affect the main observation, we temporarily only consider the case of $\phi = 0$ in the following discussion. In Figs. 1(c) and 1(d), we resolve the ionization probability to the PES at different FW intensities I_{FW}. Besides the ponderomotive shift of the ATI peaks, the populations of the different ATI peaks change distinctly with I_{FW}. The similar feature obtained in hydrogen and helium atoms indicates that there is a general mechanism of ionization reduction in two-color laser fields.

Taking hydrogen as an example, we calculate the (n, l)-resolved probabilities of excitation and ionization. The n-dependent populations are shown in the upper row of Fig. 2 for the different I_{FW} marked by the dashed lines in

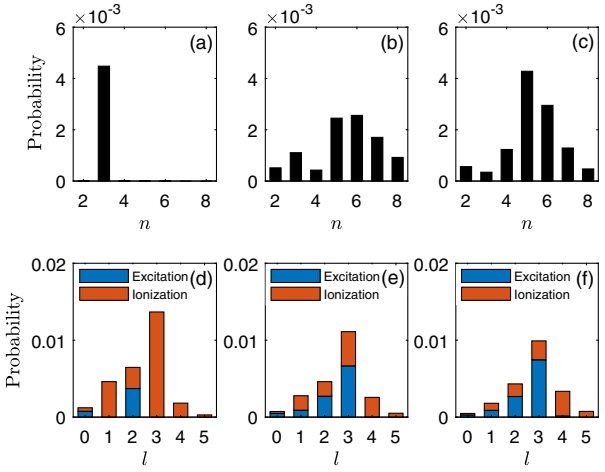

FIG. 2. Upper row (a)–(c): the n-resolved excitation probability of hydrogen. Lower row (d)–(f): the l-resolved excitation probability (blue bars) and ionization probability (red bars) of hydrogen. The SH intensity is fixed at $I_{\mathrm{SH}} = 5 \times 10^{13}$ W/cm^2, and the FW intensities are $I_{\mathrm{FW}} = 0$, 10^{12} W/cm^2 and 2.5×10^{12} W/cm^2 for the three columns from left to right.

Fig. 1(c). The lower row of Fig. 2 presents the l-resolved populations for excitation and ionization. The quantum states with $n > 8$ or $l > 5$ are not counted since their contributions are tiny. The propensity rule [38,39] in a single-photon transition and the random walking in multiphoton excitation [40,41] determine the l distribution. Combining the two panels of Figs. 2(a) and 2(d), in which only the SH is applied, and following the energy and angular momentum conservation laws, we conclude that the hydrogen atom can be excited onto the quantum state $n = 3$ by absorbing $4\omega_{\mathrm{SH}}$ and the accordingly angular partial wave is primarily distributed on the $l = 2$ state. If the atom absorbs more than $4\omega_{\mathrm{SH}}$, the electron gets freed. The maximum probability of the $l = 3$ continuum states is mainly contributed by the lowest ATI peak by absorbing $5\omega_{\mathrm{SH}}$.

The introduction of the FW severely changes the interaction process. By gradually increasing I_{FW}, the excited states with more different n are populated, which is consistent with the enhancement of excitation as shown in Fig. 1(a). The most distinct phenomenon induced by the FW is that the $l = 3$ partial wave is significantly swapped from the continuum state to the bound state, as shown in Fig. 2(e). This phenomenon is coincident with the rapid decline of the first ATI peak probability shown in Fig. 1(c). The population swap only happens when the two-color laser pulses overlap each other, which has been tested by running simulations using time-orderly two-color lasers whereas no ionization reduction is observed. When the FW intensity increases up to 2.5×10^{12} W/cm^2, shown in Fig. 2(f), the ionization probability for the $l = 3$ state continues decreasing, while the $l = 4$ state keeps increasing. The decrement in the $l = 3$ state leads to the decline of the first ATI peak and the increment on the $l = 4$ state contributes to the enhancement of the second ATI peak in Fig. 1(c).

Based on the simulation results, we may deduce the multiphoton ionization reduction in the two-color laser pulses. The ionization processes at different I_{FW} are sketched in Fig. 3. When only the SH is switched on, the ionization process is neat and simple, i.e., the hydrogen atom directly absorbs multiple photons by passing the near-resonant $3s$ and $3d$ states, as sketched in Fig. 3(a). According to the propensity rule [38,39], the population on the $3d$ state is larger than that on the $3s$ state. When the FW is added with $I_{\mathrm{FW}} = 10^{12}$ W/cm^2, as presented in Fig. 3(b), the hydrogen may absorb several ω_{SH} and one ω_{FW} simultaneously. Since the energies of Rydberg states are almost continuous, some Rydberg states can be resonantly launched by absorbing $4\omega_{\mathrm{SH}} + \omega_{\mathrm{FW}}$. For the (n, f) states, which have the largest population as presented in Fig. 2(e), though they are very weakly bound, the electron in these states has very large orbitals and thus stands off the nuclei, leading to the inefficiency of absorbing extra ω_{SH} and thus the reduction of main ATI peaks in Fig. 1(c). Such orbital stabilization will be discussed quantitatively a bit later. With the further increase of the FW intensity, as sketched in Fig. 3(c), the direct pathway of absorbing $5\omega_{\mathrm{SH}}$ is further reduced, and the temporary populations in (n, f) states are so large that their further absorption of another ω_{FW} or ω_{SH} is noticeable, contributing to the first and second ATI peaks in Fig. 1(c). Since these two ATI peaks are achieved by totally absorbing six photons, the corresponding partial wave number mainly distributes on $l = 4$, as shown in Fig. 2(f). If the FW is even stronger, multiple ω_{FW} will participate in the excitation and ionization processes, and even change the ionization from

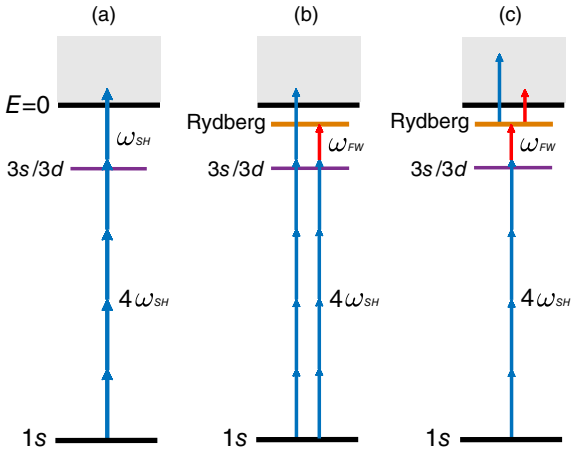

FIG. 3. Sketches of ionization when the FW with different intensities are switched on. The SH intensity is fixed at $I_{\mathrm{SH}} = 5 \times 10^{13}$ W/cm^2, and the FW intensities are $I_{\mathrm{FW}} = 0$, 10^{12} W/cm^2 and 2.5×10^{12} W/cm^2 for the panels (a)–(c), respectively.

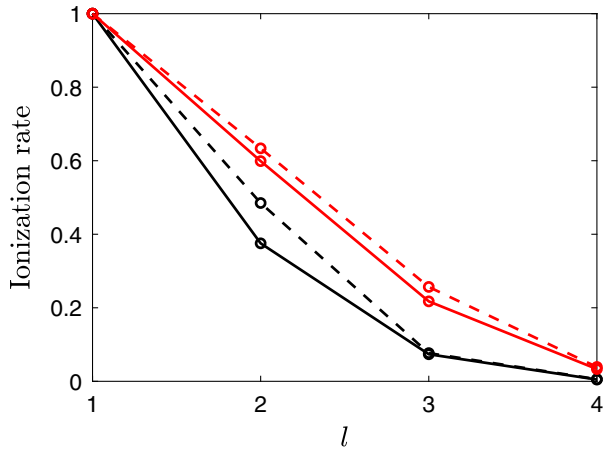

FIG. 4. The l-dependent ionization rate of the $n = 5$ Rydberg state. The solid lines are calculated with the first-order perturbation theory, and the dashed lines are obtained by solving the TDSE. The results for the sole SH and FW are indicated by the black and red lines, respectively. The SH and FW intensities are $I_{\mathrm{SH}} = 10^{13}$ W/cm^2 and $I_{\mathrm{FW}} = 10^{12}$ W/cm^2.

multiphoton to tunneling regimes. Since different ATI peaks are generated by different pathways, their time information of ionization should be different and can be extracted by phase-of-phase spectroscopy [21,42].

In the above analysis, the FW intensity determines the tug-of-war between excitation and ionization. Such a scenario also relies on the unique property of the Rydberg states. For the single-photon ionization, we calculate the ionization rate of Rydberg states $(n, l) = (5, l)$ using the first-order perturbation theory [43]. Alternatively, we directly solve the TDSE by starting from the initial state $(5, l)$ and obtain the ionization rate. Figure 4 shows the l-dependent ionization rates. All data have been normalized by the values at $l = 1$. The ionization rates monotonically decrease with the increase of l, and such descent is more distinct for absorbing ω_{SH}. For example, the dipole-transition rates for $l = 4$ are about 0.5% and 3% of those of $l = 1$ if driven by the sole SH and FW, respectively. This confirms the stabilization of (n, f) states sketched in Fig. 3.

To demonstrate our theoretical expectations, an experimental study on the ionization of helium atoms in the proposed two-color laser fields is performed with velocity map imaging (VMI) spectroscopy. A linearly polarized femtosecond laser pulse (35 fs, 800 nm, 1 kHz) delivered from a Ti:sapphire amplifier is collimated into a piece of 200 μm thick β-barium borate (BBO) crystal to generate the SH. The SH is separated from the FW whose intensity and polarization can be adjusted independently. The SH arm is employed by a motorized delay stage for temporal synchronization with respect to its FW. Stabilization is implemented for the relative phase between the two colors by sending a beam of continuum-wave laser at 633 nm inside the interferometer and providing feedback control on a piezo delay stage on one arm. The linearly polarized two-color pulses are collinearly recombined and the relative phase shift is finely tuned by a pair of wedges. The two-color pulses are then sent into the VMI chamber, to be focused to ionize helium atoms. The focusing mirror is a concave reflection mirror with $f = 75$ mm inside the chamber. In this experiment, the SH intensity is calibrated by the ionization of Ar atoms [44], which is fixed at about 1.5×10^{14} W/cm^2. The FW intensity can be finely tuned by a neutral density filter.

The measured He^+ yield in the two-color field as a function of I_{FW} is shown in Fig. 5(a). For comparison, in Fig. 5(b), we present the simulation results by considering the focal-volume intensity averages of the two-color laser pulses [45]. In both panels, the yields have been normalized by their values at $I_{\mathrm{FW}} = 0$. Both curves show similar ionization reduction. The remaining discrepancy, for example, the location of the minima, is mainly attributed to the uncertainty of the laser intensity characterization in our experiment. Moreover, the measured and simulated ionization probabilities of helium as a function of the relative phase are shown in Figs. 5(c) and 5(d), where I_{FW} are fixed at 1.6×10^{12} W/cm^2 and 10^{12} W/cm^2, respectively. In both panels, all data have been normalized by their own minima. One may clearly see the ionization fluctuation with a period of 0.5π. As we discussed above, the SH-FW laser fields bring the atoms into the $l = 3$ state by two pathways. The first pathway is the direct ionization of the absorption of five SH photons, and the other one is the

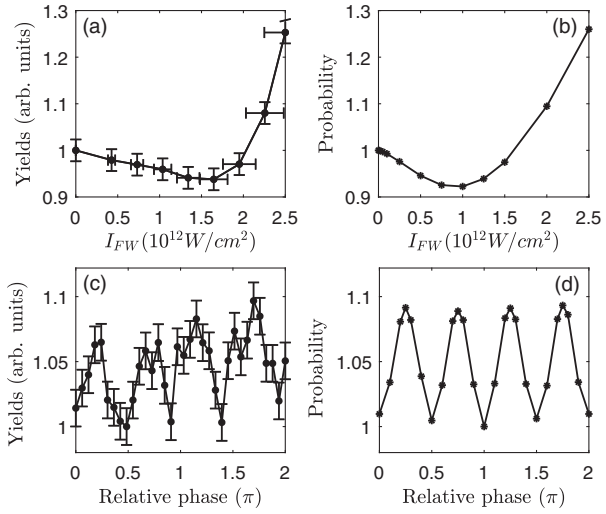

FIG. 5. Upper row: the measured (a) and simulated (b) ionization probabilities of helium as a function of the FW intensity. Lower row: the measured (c) and simulated (d) ionization probabilities of helium as a function of the relative phase between the SH and FW pulses. The simulations are obtained by taking account of the focal-volume intensity averages. The SH intensities in both the experiment and simulation are 1.5×10^{14} W/cm^2, and the FW intensities are fixed at 1.6×10^{12} W/cm^2 (c) and 10^{12} W/cm^2 (d), respectively.

excitation into Rydberg states by absorbing four SH photons and a FW photon, followed by the ionization of further absorbing another FW photon. The interference of these two pathways induces the fluctuation presented in Figs. 5(c) and 5(d). Though the relative phase ϕ modifies the ionization probability, the overall ionization probability is consistently reduced regardless of ϕ.

In conclusion, the mechanism of ionization reduction in strong laser fields is explored. Once an atom is exposed to the SH-FW laser fields, the weak FW shunts the wave packet to Rydberg states with large l, which are, though loosely bound, hard to ionize. By regulating the FW intensity, the populations on Rydberg states and continuum states can be allotted, and the minimum ionization probability can be achieved if the FW intensity is in the order of 10^{12} W/cm^2 regardless of the relative phase between the two colors. Our experimental measurement confirms the ionization reduction. Our study provides an alternatively successful scheme of ionization control.

This work was supported by National Natural Science Foundation of China (NSFC) (Grants No. 11925405, No. 11721091, No. 91850203, No. 11764041, No. 92050105, and No. 11834004), National Key R&D Program of China (Grants No. 2018YFA0404802 and No. 2018YFA0306303), the Scientific Research Program of the Higher Education Institution of Xinjiang, China (Grant No. XJEDU2021Y049). Simulations were performed at Shanghai Jiao Tong University.

*hli@lps.ecnu.edu.cn
†fhe@sjtu.edu.cn

[1] P. B. Corkum, Phys. Rev. Lett. **71**, 1994 (1993).
[2] J. L. Krause, K. J. Schafer, and K. C. Kulander, Phys. Rev. Lett. **68**, 3535 (1992).
[3] M. Protopapas, C. H. Keitel, and P. L. Knight, Rep. Prog. Phys. **60**, 389 (1997).
[4] J.-L. Xu, C. I. Blaga, A. D. DiChiara, E. Sistrunk, K.-K. Zhang, Z.-J. Chen, Anh-Thu Le, T. Morishita, C.-D. Lin, P. Agostini, and L. F. DiMauro, Phys. Rev. Lett. **109**, 233002 (2012).
[5] A. Rudenko *et al.*, Nature (London) **546**, 129 (2017).
[6] M. F. Kling, C. Siedschlag, A. J. Verhoef, J. I. Khan, M. Schultze, T. Uphues, Y. Ni, M. Uiberacker, M. Drescher, F. Krausz, and M. J. J. Vrakking, Science **312**, 246 (2006).
[7] F. He, C. Ruiz, and A. Becker, Phys. Rev. Lett. **99**, 083002 (2007).
[8] M. Kunitski, N. Eicke, P. Huber, J. Köhler, S. Zeller, J. Voigtsberger, N. Schlott, K. Henrichs, H. Sann, F. Trinter, L. Ph. H. Schmidt, A. Kalinin, M. S. Schöffler, T. Jahnke, M. Lein, and R. Dörner, Nat. Commun. **10**, 1 (2019).
[9] L. V. Keldysh, Sov. Phys. JETP **20**, 1307 (1965).
[10] F. Yergeau, G. Petite, and P. Agostini, J. Phys. B **19**, L663 (1986).
[11] M. Uiberacker, Th. Uphues, M. Schultze, A. J. Verhoef, V. Yakovlev, M. F. Kling, J. Rauschenberger, N. M. Kabachnik, H. Schröder, M. Lezius, K. L. Kompa, H.-G. Muller, M. J. J. Vrakking, S. Hendel, U. Kleineberg, U. Heinzmann, M. Drescher, and F. Krausz, Nature (London) **446**, 627 (2007).
[12] S. Augst, D. Strickland, D. D. Meyerhofer, S. L. Chin, and J. H. Eberly, Phys. Rev. Lett. **63**, 2212 (1989).
[13] T. Brixner, N. H. Damrauer, and G. Gerber, Adv. At. Mol. Opt. Phys. **46**, 1 (2001).
[14] M. Wollenhaupt, V. Engel, and T. Baumert, Annu. Rev. Phys. Chem. **56**, 25 (2005).
[15] S. Kerbstadt, K. Eickhoff, T. Bayer, and M. Wollenhaupt, Adv. Phys. **4**, 1672583 (2019).
[16] A. Palacios and F. Martín, WIREs Comput. Mol. Sci. **10**, e1430 (2020).
[17] S. Eckart, K. Fehre, N. Eicke, A. Hartung, J. Rist, D. Trabert, N. Strenger, A. Pier, L. Ph. H. Schmidt, T. Jahnke, M. S. Schöffler, M. Lein, M. Kunitski, and R. Dörner, Phys. Rev. Lett. **121**, 163202 (2018).
[18] X.-C. Gong, P.-L. He, Q.-Y. Song, Q.-Y. Ji, H.-F. Pan, J.-X. Ding, F. He, H.-P. Zeng, and J. Wu, Phys. Rev. Lett. **113**, 203001 (2014).
[19] D. G. Arbó, C. Lemell, S. Nagele, N. Camus, L. Fechner, A. Krupp, T. Pfeifer, S. D. López, R. Moshammer, and J. Burgdörfer, Phys. Rev. A **92**, 023402 (2015).
[20] M. Richter, M. Kunitski, M. Schöffler, T. Jahnke, L. P. H. Schmidt, M. Li, Y.-Q. Liu, and R. Dörner, Phys. Rev. Lett. **114**, 143001 (2015).
[21] S. Skruszewicz, J. Tiggesbäumker, K.-H. Meiwes-Broer, M. Arbeiter, Th. Fennel, and D. Bauer, Phys. Rev. Lett. **115**, 043001 (2015).
[22] X.-C. Gong, C. Lin, F. He, Q.-Y. Song, K. Lin, Q.-Y. Ji, W.-B. Zhang, J.-Y. Ma, P.-F. Lu, Y.-Q. Liu, H.-P. Zeng, W.-F. Yang, and J. Wu, Phys. Rev. Lett. **118**, 143203 (2017).
[23] M. Li, H. Xie, W. Cao, S.-Q. Luo, J. Tan, Y.-D. Feng, B.-J. Du, W.-Y. Zhang, Y. Li, Q.-B. Zhang, P.-F. Lan, Y.-M. Zhou, and P.-X. Lu, Phys. Rev. Lett. **122**, 183202 (2019).
[24] J.-W. Geng, W.-H. Xiong, X.-R. Xiao, L.-Y. Peng, and Q.-H. Gong, Phys. Rev. Lett. **115**, 193001 (2015).
[25] C. A. Mancuso, K. M. Dorney, D. D. Hickstein, J. L. Chaloupka, J. L. Ellis, F. J. Dollar, R. Knut, P. Grychtol, D. Zusin, C. Gentry, M. Gopalakrishnan, H. C. Kapteyn, and M. M. Murnane, Phys. Rev. Lett. **117**, 133201 (2016).
[26] L. J. Zipp, A. Natan, and P. H. Bucksbaum, Optica **1**, 361 (2014).
[27] M. Bertolino and J. M. Dahlström, Phys. Rev. Res. **3**, 013270 (2021).
[28] Y.-D. Feng, M. Li, S.-Q. Luo, K. Liu, B.-J. Du, Y.-M. Zhou, and P.-X. Lu, Phys. Rev. A **100**, 063411 (2019).
[29] S. D. López, S. Donsa, S. Nagele, D. G. Arbó, and J. Burgdörfer, Phys. Rev. A **104**, 043113 (2021).
[30] M. Han, P.-P. Ge, Y. Shao, Q.-H. Gong, and Y.-Q. Liu, Phys. Rev. Lett. **120**, 073202 (2018).
[31] P. M. Paul, E. S. Toma, P. Breger, G. Mullot, F. Augé, P. Balcou, H. G. Muller, and P. Agostini, Science **292**, 1689 (2001).
[32] X.-M. Tong and C.-D. Lin, J. Phys. B **38**, 2593 (2005).
[33] H. Bachau, E. Cormier, P. Decleva, J. E. Hansen, and F. Martín, Rep. Prog. Phys. **64**, 1815 (2001).
[34] B. Fetić, W. Becker, and D. B. Milošević, Phys. Rev. A **102**, 023101 (2020).

[35] D. Bauer and P. Koval, Comput. Phys. Commun. **174**, 396 (2006).
[36] A. D. Bandrauk and H. Shen, Chem. Phys. Lett. **176**, 428 (1991).
[37] X.-S. Chen, A. Sanpera, and K. Burnett, Phys. Rev. A **51**, 4824 (1995).
[38] U. Fano, Phys. Rev. A **32**, **617** (1985).
[39] D. Busto, J. Vinbladh, S.-Y. Zhong, M. Isinger, S. Nandi, S. Maclot, P. Johnsson, M. Gisselbrecht, A. L'Huillier, E. Lindroth, and J. M. Dahlström, Phys. Rev. Lett. **123**, 133201 (2019).
[40] Z. Chen, T. Morishita, A. T. Le, M. Wickenhauser, X.-M. Tong, and C.-D. Lin, Phys. Rev. A **74**, 053405 (2006).
[41] D. Chetty, R. D. Glover, B. A. deHarak, X. M. Tong, H. Xu, T. Pauly, N. Smith, K. R. Hamilton, K. Bartschat, J. P. Ziegel, N. Douguet, A. N. Luiten, P. S. Light, I. V. Litvinyuk, and R. T. Sang, Phys. Rev. A **101**, 053402 (2020).
[42] K. Klünder, J. M. Dahlström, M. Gisselbrecht, T. Fordell, M. Swoboda, D. Guénot, P. Johnsson, J. Caillat, J. Mauritsson, A. Maquet, R. Taïeb, and A. L'Huillier, Phys. Rev. Lett. **106**, 143002 (2011).
[43] M. J. Seaton, J. Phys. B **28**, 3185 (1995).
[44] K. Henrichs, M. Waitz, F. Trinter, H. Kim, A. Menssen, H. Gassert, H. Sann, T. Jahnke, J. Wu, M. Pitzer, M. Richter, M. S. Schöffler, M. Kunitski, and R. Dörner, Phys. Rev. Lett. **111**, 113003 (2013).
[45] A. S. Alnaser, X.-M. Tong, T. Osipov, S. Voss, C. M. Maharjan, B. Shan, Z. Chang, and C. L. Cocke, Phys. Rev. A **70**, 023413 (2004).